# Supporting Information

## Figueiredo et al. 10.1073/pnas.1211614109

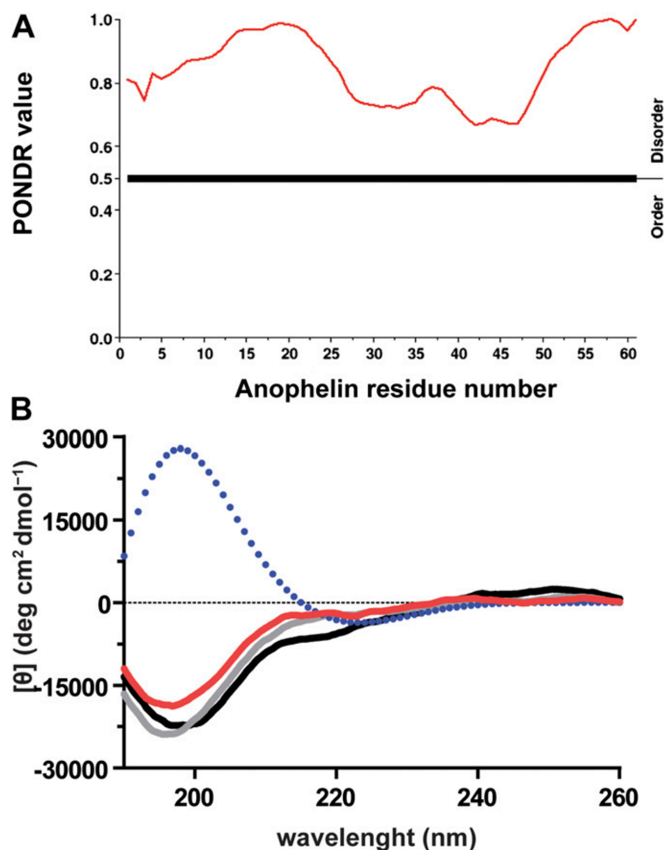


**Fig. S1.** Anophelin is intrinsically disordered in solution but structured when in complex with thrombin. (*A*) Prediction of natural disordered regions (VL-XT predictor) (1) in the primary sequence of anophelin$^{Aa}$. Residues exceeding a threshold value of 0.5 are considered disordered. Similar results are provided by other algorithms such as DisEMBL (2), GlobPlot (3), and PrDOS (4). (*B*) Experimental circular dichroism (CD) spectra of anophelin$^{Aa}$ (black), anophelin$^{1–31}$ (gray), and anophelin$^{32–61}$ (red) in water (0.025 mg/mL) are superimposed to the theoretical CD spectrum of thrombin-bound anophelin (blue; calculated with DichroCal) (5).


1. Romero P, et al. (2001) Sequence complexity of disordered protein. *Proteins* 42(1):38–48.
2. Linding R, et al. (2003) Protein disorder prediction: Implications for structural proteomics. *Structure* 11(11):1453–1459.
3. Linding R, Russell RB, Neduva V, Gibson TJ (2003) GlobPlot: Exploring protein sequences for globularity and disorder. *Nucleic Acids Res* 31(13):3701–3708.
4. Ishida T, Kinoshita K (2007) PrDOS: Prediction of disordered protein regions from amino acid sequence. *Nucleic Acids Res* 35(Web Server issue):W460–W464.
5. Bulheller BM, Hirst JD (2009) DichroCalc—circular and linear dichroism online. *Bioinformatics* 25(4):539–540.

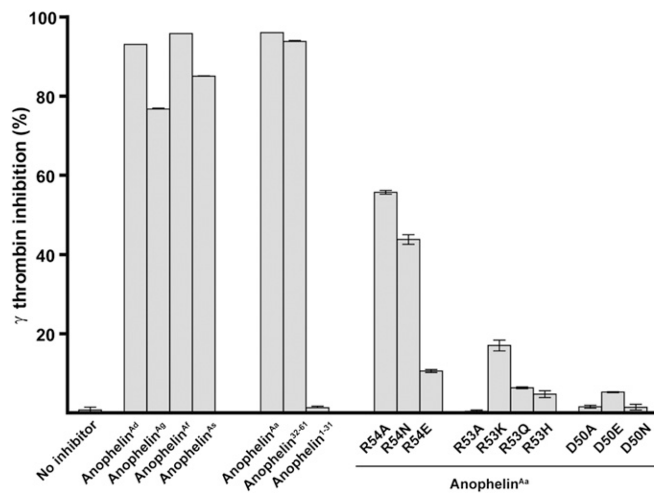


**Fig. S2.** Anophelins inhibit exosite I-disrupted γ-thrombin. γ-thrombin (5 nM) was preincubated with 5,000 nM inhibitor for 15 min. Inhibition levels (mean values ± SEM) by WT anophelins, anophelin$^{1–31}$, anophelin$^{32–61}$, and anophelin$^{Aa}$ mutants were determined by measuring the residual amidolytic activity of the proteinase against 100 μM chromogenic substrate after a 20-min reaction.

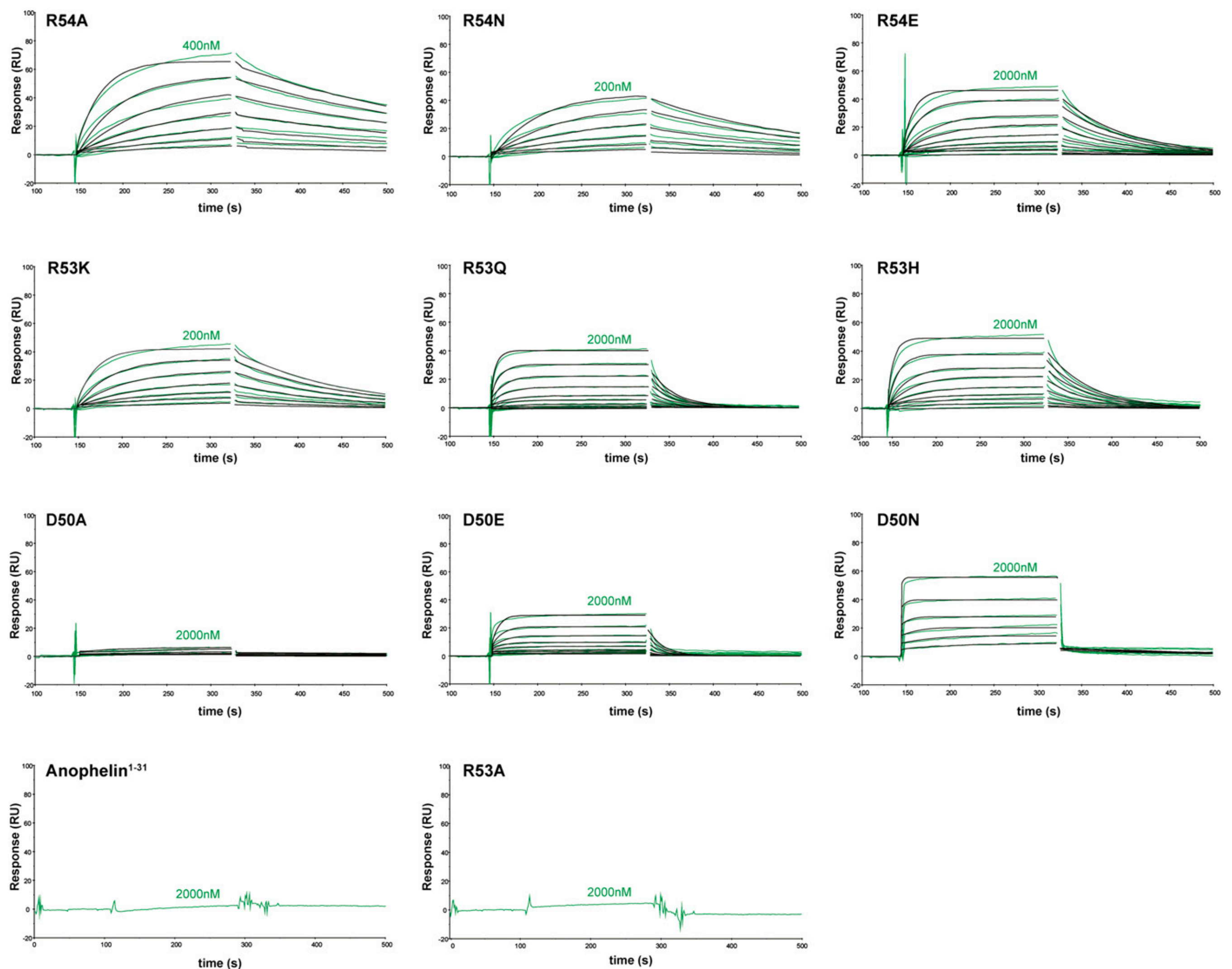


**Fig. S3.** Anophelin binding to immobilized human α-thrombin measured by surface plasmon resonance. Sensorgrams depict kinetics experiments for anophelin mutants. Each set of experimental curves (green) represents decreasing concentrations of analyte in twofold dilution steps (the highest concentration used is indicated). The black traces represent the fitted data according to the 1:1 Langmuir binding model. No residual binding was observed for R53A mutant and anophelin$^{1-31}$. RU, resonance unit.

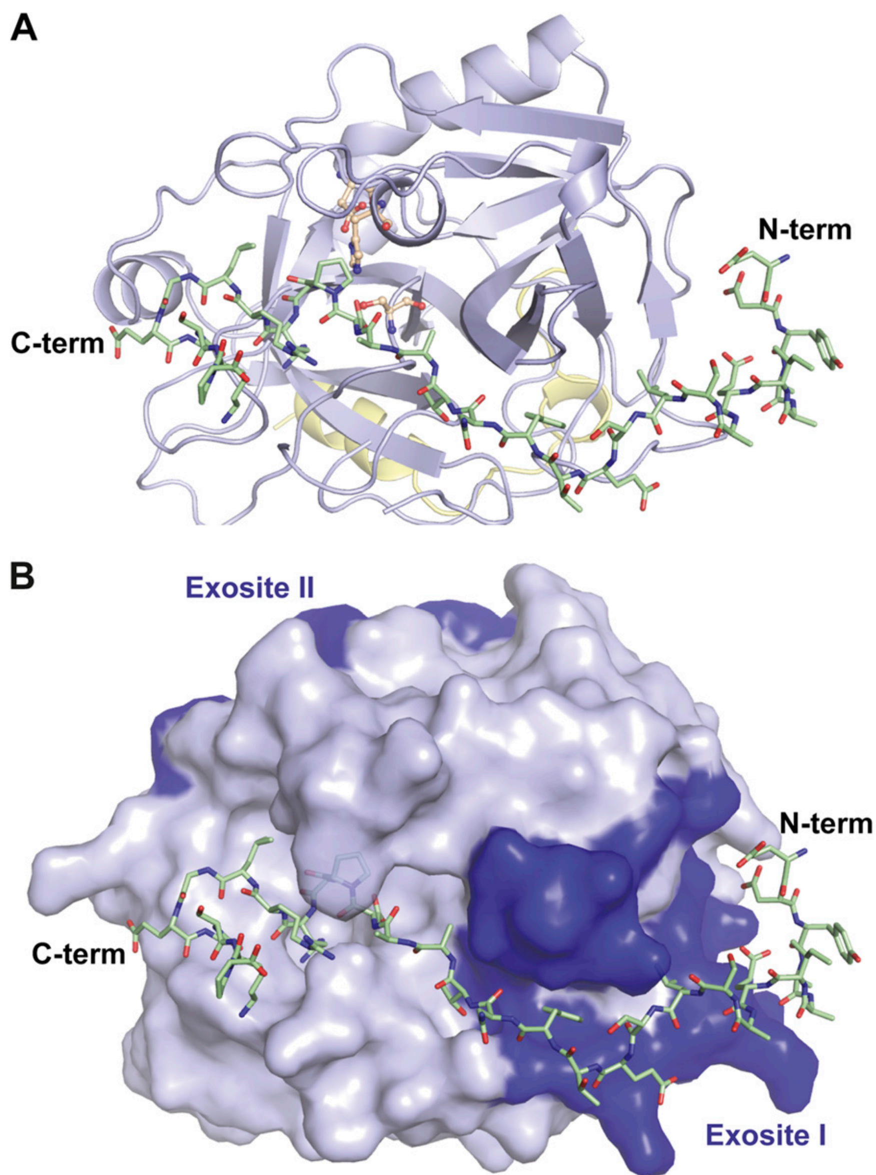


**Fig. S4.** Anophelin binds to both the active site and the exosite I of α-thrombin. (*A*) Thrombin (cartoon representation with light and heavy chains in yellow and gray, respectively) in complex with anophelin (ball and stick model with nitrogen atoms in blue, oxygen in red, and carbon in green). Active site residues are represented in ball and stick and color-coded as anophelin, except for carbon atoms (colored salmon). (*B*) Solid surface representation of thrombin (gray) with exosites I and II highlighted in blue. Bound anophelin is represented as a stick model (colored as in *A*).

PNAS PNAS PNAS

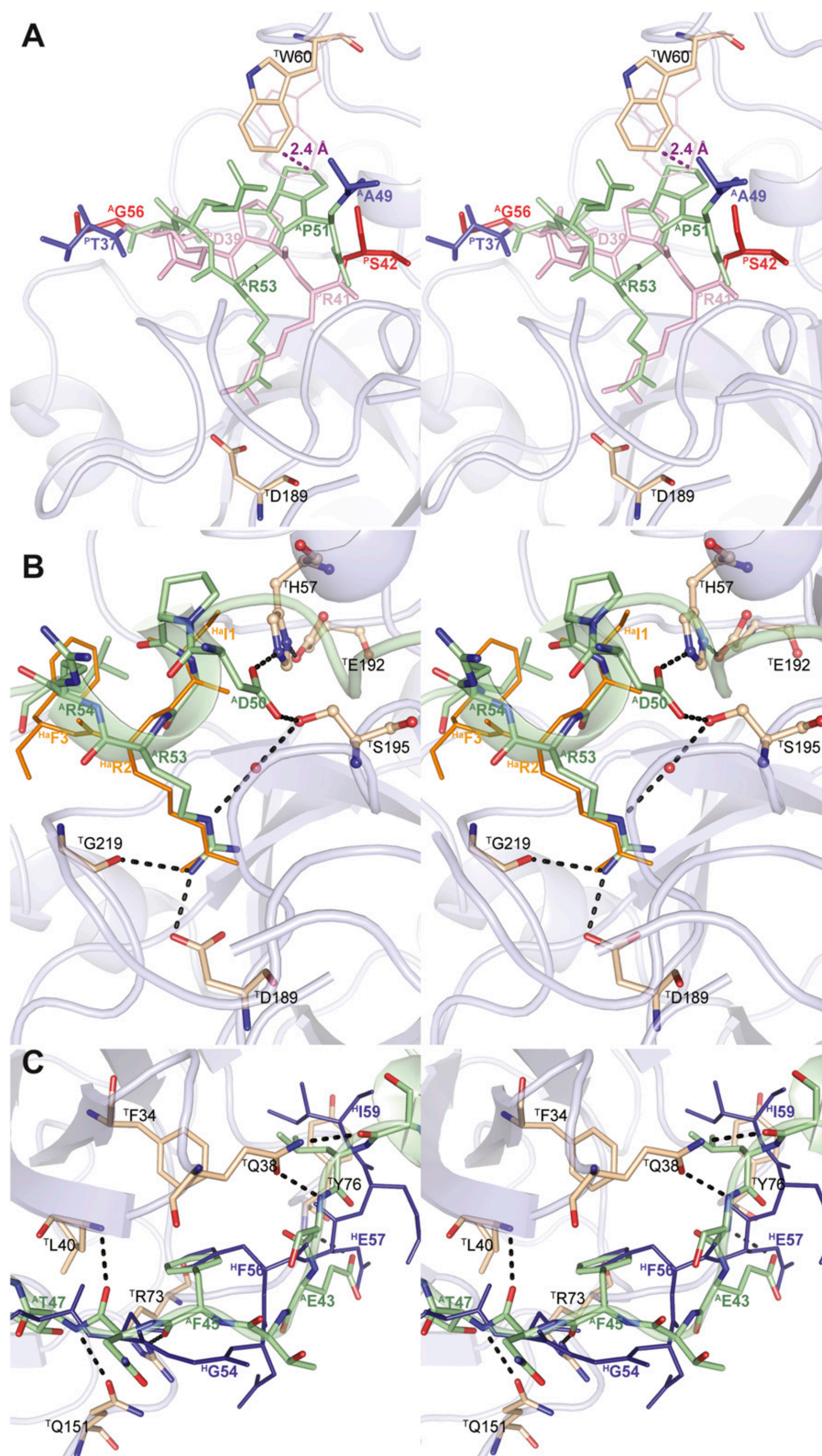


**Fig. S5.** Comparison of anophelin with thrombin substrates and inhibitors. The coordinates of the thrombin·anophelin complex are superposed to the coordinates of the (*A*) thrombin·protease-activated receptor 1 (PAR1) (1), (*B*) thrombin·haemadin (2), and (*C*) thrombin·hirudin (3) complexes. Thrombin is represented as a gray cartoon, with selected residues as color-coded sticks (nitrogen atoms in blue, oxygen in red, and carbon in salmon) and active site residues in color-coded ball-and-stick representation. Anophelin is represented in green (*A*) or color-coded [as for thrombin, except for carbon atoms (green); *B* and *C*]. Water molecules are shown as red spheres, and hydrogen bonds are represented by black dotted lines. (*A*) Despite the reversed direction of the respective peptide chains (the N-terminal residue of each segment is highlighted in blue, and the C-terminal residue is in red), several residues of anophelin and PAR1 (pink) establish equivalent interactions with the proteinase. The side chain of $^{A}$R53 occupies the $S_1$ pocket of the enzyme, similar to $^{P}$R41, despite the significant distance (4.2 Å) between their Cα atoms. The preceding $^{A}$P51 displaces the 60 loop of thrombin (2.4 Å for $^{T}$W60D CZ3 in PAR1), partially overlapping with $^{P}$P40 at binding site $S_2$. $^{A}$L55 overlaps well with $^{P}$L38 at the enzyme's aryl-binding site (Cα atoms are 1.0 Å apart). (*B*) The $^{Ha}$R2 residue of the I14 family inhibitor, haemadin (orange), occupies the $S_1$ pocket of thrombin interacting with $^{T}$D189 in a similar way to the way observed for anophelin $^{A}$R53. (*C*) The acidic

Legend continued on following page

$^{A}$E32-$^{A}$F45 segment binds to the exosite I of the enzyme, similar to the negatively charged C-terminal portion of hirudin (blue), with a number of similar interactions: the side chain of $^{A}$F45 mimics the edge-on stacking with $^{T}$F34 observed for $^{H}$F56, despite the 4.4-Å distance between their Cα atoms, whereas the main-chain nitrogen of $^{T}$Y76 donates an hydrogen bond to the side chain of $^{A}$E43 or $^{H}$E57.


1. Gandhi PS, Chen Z, Di Cera E (2010) Crystal structure of thrombin bound to the uncleaved extracellular fragment of PAR1. *J Biol Chem* 285(20):15393–15398.
2. Richardson JL, et al. (2000) Crystal structure of the human α-thrombin-haemadin complex: An exosite II-binding inhibitor. *EMBO J* 19(21):5650–5660.
3. Liu CC, Brustad E, Liu W, Schultz PG (2007) Crystal structure of a biosynthetic sulfo-hirudin complexed to thrombin. *J Am Chem Soc* 129(35):10648–10649.


**Table S1. Anophelin binding increases the stability of human α-thrombin against thermal denaturation**

| | Concentration (μM) | | | | |
|---|---|---|---|---|---|
| Inhibitor | 1 | 7.25 | 12.5 | 25 | 50 |
| Anophelin$^{Ad}$ | 53.00 ± 0.50 | 61.00 ± 0.50 | 62.50 ± 0.50 | 64.25 ± 0.25 | 66.00 ± 0.00 |
| Anophelin$^{Ag}$ | 60.00 ± 0.50 | 62.25 ± 0.25 | 64.75 ± 0.25 | 66.50 ± 0.00 | 66.50 ± 0.00 |
| Anophelin$^{Af}$ | 54.75 ± 0.25 | 58.75 ± 0.25 | 60.00 ± 0.00 | 61.50 ± 0.00 | 63.75 ± 0.25 |
| Anophelin$^{As}$ | 52.75 ± 0.25 | 57.75 ± 0.75 | 59.50 ± 0.00 | 60.75 ± 0.25 | 61.50 ± 0.25 |
| Anophelin$^{Aa}$ | 59.25 ± 0.25 | 62.50 ± 0.00 | 65.00 ± 0.00 | 65.50 ± 0.50 | 68.00 ± 0.00 |
| Anophelin$^{32–61}$ | 52.50 ± 0.00 | 60.00 ± 0.00 | 62.25 ± 0.25 | 64.00 ± 0.00 | 65.00 ± 0.00 |
| Anophelin$^{1–31}$ | 53.25 ± 0.25 | 53.25 ± 0.25 | 53.00 ± 0.00 | 53.50 ± 0.00 | 53.50 ± 0.00 |
| Anophelin$^{Aa}$ R54A | 56.50 ± 0.00 | 60.75 ± 0.25 | 62.00 ± 0.25 | 63.00 ± 0.50 | 64.50 ± 0.00 |
| Anophelin$^{Aa}$ R54N | 51.50 ± 0.00 | 58.00 ± 0.50 | 59.00 ± 0.00 | 60.50 ± 0.50 | 61.00 ± 0.00 |
| Anophelin$^{Aa}$ R54E | 54.00 ± 0.00 | 57.25 ± 0.25 | 58.50 ± 0.00 | 59.50 ± 0.00 | 60.50 ± 0.00 |
| Anophelin$^{Aa}$ R53A | 52.50 ± 0.00 | 52.50 ± 0.00 | 52.50 ± 0.00 | 53.00 ± 0.00 | 53.50 ± 0.00 |
| Anophelin$^{Aa}$ R53K | 53.00 ± 2.00 | 58.25 ± 0.25 | 59.75 ± 0.25 | 61.00 ± 0.00 | 62.00 ± 0.00 |
| Anophelin$^{Aa}$ R53Q | 53.00 ± 0.00 | 54.25 ± 1.25 | 56.50 ± 0.00 | 57.50 ± 0.00 | 58.40 ± 0.40 |
| Anophelin$^{Aa}$ R53H | 53.50 ± 0.00 | 56.50 ± 0.00 | 57.50 ± 0.00 | 58.50 ± 0.00 | 59.25 ± 0.25 |
| Anophelin$^{Aa}$ D50A | 48.50 ± 0.00 | 50.00 ± 0.00 | 51.50 ± 0.00 | 53.25 ± 0.25 | 54.50 ± 0.00 |
| Anophelin$^{Aa}$ D50E | 50.25 ± 0.25 | 52.50 ± 0.00 | 55.75 ± 0.25 | 57.00 ± 0.00 | 58.50 ± 0.00 |
| Anophelin$^{Aa}$ D50N | 50.50 ± 0.00 | 51.50 ± 0.00 | 53.75 ± 0.25 | 53.75 ± 0.25 | 55.00 ± 0.00 |

Thrombin stability to thermal denaturation was measured in the presence of increasing molar ratios of anophelin variants by differential scanning fluorimetry. Melting temperatures ($T_m$) were determined as the inflection points of the experimental curves and are given as mean values ± SD. In the absence of inhibitor, thrombin displays a $T_m$ of 52.50 ± 0.50 °C.